Chemical Science

ROYAL SOCIETY OF CHEMISTRY

EDGE ARTICLE

View Article Online
View Journal | View Issue

Check for updates

Cite this: *Chem. Sci.*, 2020, **11**, 7991

All publication charges for this article have been paid for by the Royal Society of Chemistry

Received 16th June 2020
Accepted 9th July 2020

DOI: 10.1039/d0sc03336g

rsc.li/chemical-science

Engineering a highly selective probe for ratiometric imaging of H_2S_n and revealing its signaling pathway in fatty liver disease†

Wei Li,‡[a] Lu Wang,‡[b] Shulu Yin,[a] Huanhua Lai,[a] Lin Yuan *[a] and Xiaobing Zhang [a]

Hydrogen polysulfides (H_2S_n, $n > 1$) have continuously been proved to act as important signal mediators in many physiological processes. However, the physiological role of H_2S_n and their signaling pathways in complex diseases, such as the most common liver disease, nonalcoholic fatty liver disease (NAFLD), have not been elucidated due to lack of suitable tools for selective detection of intracellular H_2S_n. Herein, we adopted a general and practical strategy including recognition site screening, construction of a ratiometric probe and self-assembly of nanoparticles, to significantly improve the probes' selectivity, photostability and biocompatibility. The ratiometric probe **PPG-Np-RhPhCO** selectively responds to H_2S_n, avoiding interaction with biothiol and persulfide. Moreover, this probe was applied to image H_2S_n in NAFLD for the first time and reveal the H_2S_n generation pathways in the cell model of drug-treated NAFLD. The pathway of H_2S_n revealed by **PPG-Np-RhPhCO** provides significant insights into the roles of H_2S_n in NAFLD and future drug development.

Introduction

Hydrogen sulfide, one of the reactive sulfur species (RSS), has proved to be a key molecule in many diseases.[1,2] Studies have shown that H_2S and H_2S_n are redox partners in terms of chemical properties and coexist in biological systems.[3,4] Recently, accumulated data have indicated the important roles of H_2S_n in signal transduction in physiological processes, such as cardiovascular system, ion channels, oxidative post-translational modification, antioxidation and cytoprotection.[5–11] Furthermore, aberrant production and physiological levels of H_2S_n are found to be correlated with physiological processes and diseases such as sulfur redox balance and liver disease.[12,13] Nonalcoholic fatty liver disease (NAFLD), referring to a wide spectrum of liver damage that ranges from simple steatosis to steatohepatitis, advanced fibrosis, and cirrhosis, represents the most common chronic liver disease in developed countries. Clarification of the functions of signaling molecules in NAFLD offers important insights into the pathogenesis of the disease, drug development and therapeutic evaluation.[14,15] Even though some research studies have implied the existence of H_2S_n in liver disease,[12,16,17] the role and signaling pathway of H_2S_n in the process of NAFLD have not been revealed due to the lack of suitable analytical methods for selectively monitoring H_2S_n in living biological systems.

Some *in vitro* analysis techniques including UV-spectroscopy, cold cyanolysis and mass spectrometry have been described to detect H_2S_n,[5,18] while fluorescence imaging has received widespread attention in H_2S_n bioanalysis due to its unique advantages in live cell imaging, such as excellent biocompatibility and high spatial and temporal resolution.[19] Previous efforts in designing H_2S_n fluorescent probes were mainly based on conjugating functional groups, such as 2-fluoro-5-nitro-benzoic ester, phenyl-2-(benzoylthio)benzoate, and cinnamate ester, with hydroxyl-containing fluorophores.[4,20,21] However, these functional groups may also react with abundant biothiols and active hydrolases inside cells, which could cause interference in H_2S_n detection. Only a few probes have been designed based on other electrophilic receptors, such as derivatives of xanthene or silicon-rhodamines.[22–24] However, there are currently no methods suitable for selectively sensing H_2S_n from other persulfides (RSSH). At the same time, poor solubility, concentration fluctuation and unsatisfactory photostability make it more difficult to accurately monitor the changes of H_2S_n in live-cell imaging. To address these problems, we report a first-generation through-bond energy transfer (TBET) ratiometric fluorescent probe, **PPG-Np-RhPhCO**, with significantly improved photostability, selectivity and biocompatibility for monitoring intracellular H_2S_n *via* a simple and general strategy. The design concept consists of three steps (Fig. 1): (i) screening of new recognition sites based on the

[a]State Key Laboratory of Chemo/Biosensing and Chemometrics, College of Chemistry and Chemical Engineering, Hunan University, Changsha 410082, P. R. China. E-mail: lyuan@hnu.edu.cn

[b]Department of Chemical Biology, Max Planck Institute for Medical Research, Jahnstrasse 29, Heidelberg 69120, Germany

† Electronic supplementary information (ESI) available. See DOI: 10.1039/d0sc03336g

‡ These authors contributed equally to this work.

Open Access Article. Published on 09 July 2020. Downloaded on 2/24/2026 1:23:28 AM. This article is licensed under a Creative Commons Attribution-NonCommercial 3.0 Unported Licence.

Open Access Article. Published on 09 July 2020. Downloaded on 2/24/2026 1:23:28 AM.
This article is licensed under a Creative Commons Attribution-NonCommercial 3.0 Unported Licence.

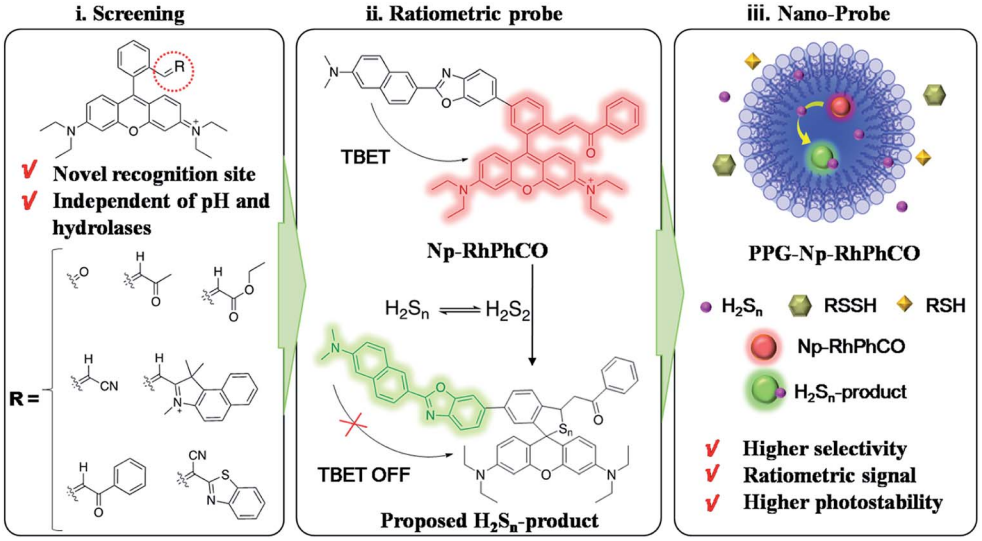

Fig. 1 Design strategy of the ratiometric fluorescent probe **PPG-Np-RhPhCO** for sensing H_2S_n. (i) Screening of new recognition sites, (ii) construction of the TBET-based ratiometric fluorescent probe for quantifying H_2S_n, (iii) self-assembly of nanoparticles to achieve high selectivity, photostability and biocompatibility.

stable electrophilic receptor, enabling an optimal response site for specific detection of H_2S_n that is independent of pH and hydrolases; (ii) construction of ratiometric probes, achieving accurate detection of H_2S_n by single-wavelength excitation; (iii) self-assembly of nanoparticles, improving the selectivity, photostability and water solubility. The nano-probe **PPG-Np-RhPhCO** was successfully applied for monitoring the generation of H_2S_n in NAFLD, which to our knowledge is reported for the first time. Importantly, we also show that 3-mercaptopyruvate sulfurtransferase (MPST) and cystathionine γ-lyase (CSE) are largely responsible for participating in the regulation of H_2S_n. Furthermore, we revealed that ROS/H_2S/H_2S_n crosstalk signaling pathways that increased ROS in the drug-treated NAFLD model would stimulate MPST and CSE to produce more H_2S, which causes significant enhancement of H_2S_n *via* reaction with ROS or catalysis by MPST and CSE.

Results and discussion

Design and screening of recognition sites

Although several fluorescent probes for H_2S_n were prepared based on the introduction of aromatic ester groups into fluorophores,[12,20,21,25,26] their poor stability resulting from the susceptibility to pH and hydrolase could easily cause false signals, thereby limiting their application in live-cell imaging. Several persulfide probes based on xanthene derivatives that are susceptible to nucleophilic attack and regulate the fluorescence changes for hydropolysulfide detection have been reported,[22–24] but they lack the specificity of H_2S_n. To address these concerns, unsaturated double bonds containing different electron-withdrawing groups were introduced into the benzene moiety of xanthene dyes (Fig. 1 and Scheme S1†). It was proposed that the reaction with H_2S_n produces persulfide intermediates *via* nucleophilic addition and then rapidly undergo intramolecular spirocyclization because of the high nucleophilicity and bis-nucleophiles of persulfide intermediates.[27] As a proof of concept, seven xanthene derivatives bearing different substituents containing unsaturated double bonds (**RhCHO1**, **RhIndo2**, **RhThia3**, **RhCN4**, **RhCOOEt5**, **RhPhCO6**, and **RhAton7** in Scheme S2†) were synthesized and tested as candidates for new recognition site screening. To examine the fluorescence response toward different RSS, S_8, $S_2O_3^{2-}$, SO_3^{2-}, HSO_3^-, SO_4^{2-}, Na_2S, GSH, Cys, Hcy, Na_2S_2 and Na_2S_4 were incubated with the probe in phosphate buffer (25 mM PBS mixed with 1% MeCN, pH 7.4) separately (Fig. 2, S1 and S2†). **RhPhCO6** was chosen as the target recognition site due to fast response to H_2S_n (<1 min, Fig. S3a†) and resistance to pH (pH 4.0–11.0, Fig. S3b†). The higher reaction activity of **RhPhCO6** toward H_2S_n than of the other six compounds was further explained by density functional theory (DFT) calculations (Fig. 2 and S4†), and it was a result of proper electrostatic charges of the β-carbon of the C=C bond and the medial carbon of rhodamine in **RhPhCO6**, as well as steric hindrance. The reaction between unsaturated double bonds and H_2S_n was followed by rapid intramolecular spirocyclization (Fig. S5†), as evidenced in the high resolution mass spectrum (Fig. S6†) and ^{1}H NMR spectrum (Fig. S7†). Furthermore, to examine the possible reasons for the specific response of **RhPhCO6** towards H_2S_n rather than H_2S, time-dependent ^{1}H NMR spectra of the reaction between **RhPhCO6** and H_2S_n or H_2S were recorded (Fig. S7 and S8†). The excellent selectivity is due to the ultra-fast reaction between **RhPhCO6** and H_2S_n, which is probably caused by the special alpha effect of H_2S_n.[18,28] Even novel recognition sites in **RhPhCO6** exhibit excellent response towards H_2S_n, but a reaction with a high concentration of GSH and Cys could cause some interference with intracellular H_2S_n sensing. Therefore, the self-assembly strategy of amphiphilic polymers was further utilized to increase the selectivity, which will be detailed in the next paragraph.

This journal is © The Royal Society of Chemistry 2020

Open Access Article. Published on 09 July 2020. Downloaded on 2/24/2026 1:23:28 AM.
This article is licensed under a Creative Commons Attribution-NonCommercial 3.0 Unported Licence.

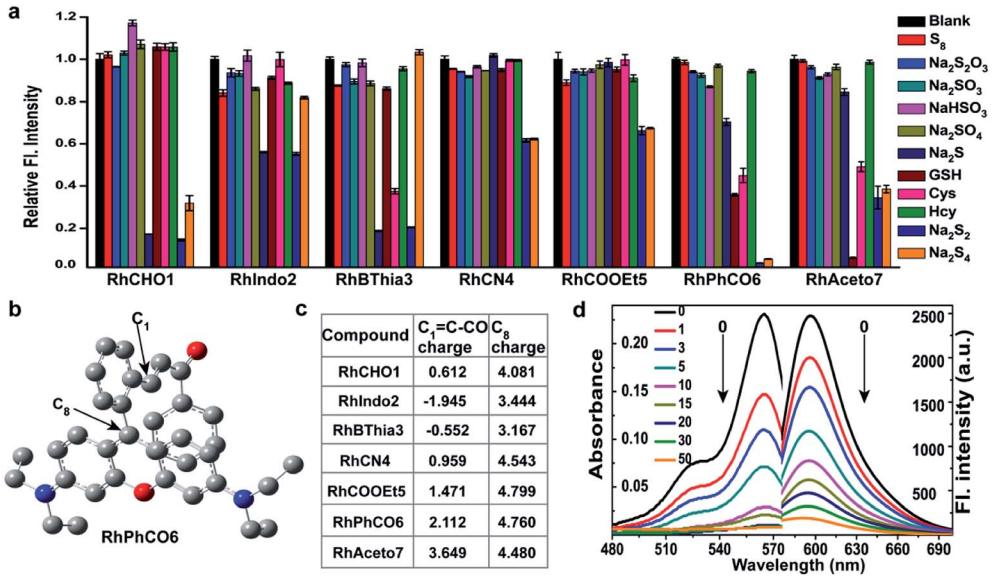

Compound	C_1=C-CO charge	C_8 charge
RhCHO1	0.612	4.081
RhIndo2	-1.945	3.444
RhBThia3	-0.552	3.167
RhCN4	0.959	4.543
RhCOOEt5	1.471	4.799
RhPhCO6	2.112	4.760
RhAceto7	3.649	4.480

Fig. 2 (a) Relative fluorescence intensities of 5 μM concentrations of compounds **RhCHO1**, **RhIndo2**, **RhBThia3**, **RhCN4**, **RhCOOEt5**, **RhPhCO6**, and **RhAceton7** in the presence of 50 μM Na_2S_2 and other biologically relevant analytes (1 mM glutathione, 50 μM Na_2S_4, and 200 μM for other analytes) in PBS (pH 7.4) at 37 °C. Incubation time: 30 min. λ_{ex} = 520 nm. (b) The structural analysis results of **RhPhCO6** *via* DFT calculations. (c) Calculated electrostatic charges of the enone β carbons C_1 = C–CO (eV) and C_8 charge (eV) of these compounds. (d) Absorption and fluorescence spectra of **RhPhCO6** (5 μM) in PBS (25 mM, pH 7.4, 1% CH_3CN, v/v) in the presence of Na_2S_2 (0–50 μM) for 5 min at 37 °C. $\lambda_{ex}/\lambda_{em}$ = 520/596 nm.

Construction of the ratiometric fluorescent nano-probe

The ratiometric signal offers more accurate detection of intracellular analytes due to its resistance to the influence of probe concentration and various cellular environments.[29–31] Several ratiometric probes for H_2S_n have been reported recently, whose ratiometric mechanisms were achieved by intramolecular charge transfer (ICT) and Förster resonance energy transfer (FRET).[12,22,32] Ratiometric probes based on through-bond energy transfer (TBET) usually exhibit higher energy transfer efficiency than those based on FRET even without spectral overlap.[33] Thus, a ratiometric fluorescent probe **Np-RhPhCO** for sensing H_2S_n was constructed by combining a naphthalene unit (donor) and **RhPhCO6** (acceptor) *via* Through-Bond Energy Transfer (TBET) cassettes (Scheme 1). The synthesis of probe **Np-RhPhCO** started from commercially available 5-bromophthalide using bromination and condensation to yield **Br-Rhod-COOH** and then reduction, oxidation and alcohol oxidation to obtain **Br-Rhod-CHO** (Scheme 1 and S3†). And the receptor **Br-RhPhCO** was subsequently synthesized *via* the classic Wittig reaction. Lastly, Pd-catalyzed Negishi cross-coupling of **Br-RhPhCO** and the boronic acid pinacol ester of Np (Np-Borate) provided the TBET-based ratiometric probe **Np-RhPhCO** (synthesis and characterization details in the ESI†). As reported before,[34] the naphthalene–rhodamine TBET platform showed two well-separated absorbance peaks at 355 nm and 565 nm with emission peaks at 486 nm and 591 nm, respectively (Fig. 3a). Titration of Na_2S_2 (0–50 μM) gradually increased the fluorescence at 486 nm and decreased the fluorescence at 591 nm, offering a 59-fold fluorescence ratio (I_{486}/I_{591}) enhancement (Fig. S9†).

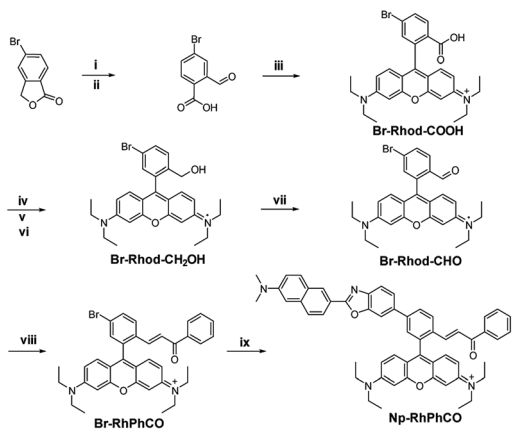

Scheme 1 Synthesis of the ratiometric probe **Np-RhPhCO**. (i) NBS, AIBN, $CHCl_3$, reflux. (ii) H_2O, reflux. (iii) *p*-Toluenesulphonic acid, propionic acid, 3-diethylaminophenol, 90 °C. (iv) H_2SO_4, CH_3OH, 80 °C. (v) $LiAlH_4$, dry THF, 0 °C. (vi) *p*-Chloranil, CH_2Cl_2/CH_3OH, rt. (vii) 1,1,1-Triacetoxy-1,1-dihydro-1,2-benziodoxol-3(1*H*)-one, CH_2Cl_2, rt. (viii) (Benzoylmethylene)triphenylphosphorane, LiCl, $CHCl_3$, 70 °C. (ix) The boronic acid pinacol ester of Np (Np-Borate), K_3PO_4, $Pd(dppf)_2Cl_2$, 1,4-dioxane/H_2O, reflux.

In recent years, nanoparticles used to improve the photostability and biocompatibility of small organic molecules have attracted increasing attention in the fields of biosensing, *in vivo* imaging and drug release.[35–38] In addition, it has been reported that the selectivity can be improved by encapsulating an organic fluorescent probe in a self-assembled supramolecular system of an amphiphilic polymer.[39] In order to achieve the application in a complex living system, we tried to encapsulate the small

Open Access Article. Published on 09 July 2020. Downloaded on 2/24/2026 1:23:28 AM.
This article is licensed under a Creative Commons Attribution-NonCommercial 3.0 Unported Licence.

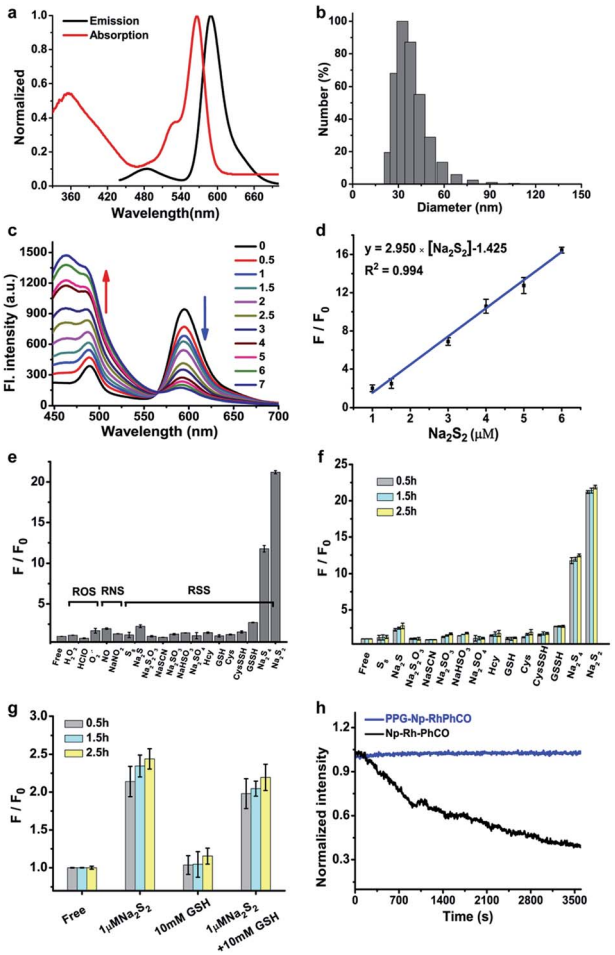

Fig. 3 (a) Absorption and fluorescence spectra of **Np-RhPhCO** (5 μM) in MeCN/PBS (v/v = 4 : 6, PBS 25 mM, pH 7.4) buffer solution at 37 °C. (b) Average hydrodynamic size of **PPG-Np-RhPhCO** measured by dynamic light scattering. (c) Fluorescence spectra of **PPG-Np-RhPhCO** (4.8 μM) in the presence of various concentrations of Na_2S_2 (0, 0.5, 1.0, 1.5, 2.0, 2.5, 3.0, 5.0, 6.0, and 7.0 μM, respectively) in PBS buffer (pH 7.4) at 37 °C. $\lambda_{ex} = 420$ nm. (d) Plot of fluorescence intensity ratio (I_{486}/I_{594}) changes as a function of Na_2S_2 concentration in PBS buffer (pH 7.4) at 37 °C. F and F_0 represent the fluorescence intensity ratio (I_{486}/I_{594}) in the presence and absence of Na_2S_2, respectively. (e) Ratiometric fluorescence changes of **PPG-Np-RhPhCO** (4.8 μM) in the presence of 7 μM Na_2S_2 and other biomolecules (1 mM glutathione, 50 μM hypochloric acid, 50 μM GSSH/CysSSH, 30 μM Na_2S_4, and 200 μM for other analytes). (f) Ratiometric fluorescence changes of **PPG-Np-RhPhCO** (4.8 μM) in the presence of 7 μM Na_2S_2 and other RSS (5 mM glutathione, 50 μM GSSH/CysSSH, 30 μM Na_2S_4, and 200 μM for other analytes) after incubation for 0.5 h, 1.5 h, and 2.5 h, respectively. (g) Ratiometric fluorescence changes of **PPG-Np-RhPhCO** (4.8 μM) in the presence of 1 μM Na_2S_2, 10 mM GSH, and the mixture of 1 μM Na_2S_2 and 10 mM GSH after incubation for 0.5 h, 1.5 h, and 2.5 h, respectively. F and F_0 represent the fluorescence intensity ratio (I_{486}/I_{594}) in the presence and absence of analytes, respectively. Measurement conditions: $\lambda_{ex} = 420$ nm, PBS (pH 7.4) buffer, 37 °C. (h) Normalized time-dependent emission profile of **PPG-Np-RhPhCO** (4.8 μM) and **Np-RhPhCO** (5 μM) with continuous irradiation for 1 h in PBS (pH = 7.4, 1% MeCN) at 37 °C using a Xe-lamp at 420 nm.

molecule ratiometric probe **Np-RhPhCO** into the self-assembled nanoparticles based on an amphiphilic copolymer to construct a more suitable organic nano-probe. 1,2-Dimyristoyl-*sn*-glycero-3-phosphoethanolamine-*N*-[methoxy(polyethylene glycol)-2000] (DSPE-PEG2000) and poly(ethylene glycol)-*block*-poly(propylene glycol)-*block*-poly(ethylene glycol) (mPEG-PPG-PEG) were applied to prepare the nano-probes, respectively (Fig. S10–13†). Among them, **PPG-Np-RhPhCO** with a 33 nm average hydrodynamic size (Fig. 3b and S12b†) exhibited a 21-fold ratiometric signal (I_{486}/I_{591}) enhancement in the presence of H_2S_n (Fig. 3c and d), displaying a better response than DSPE-Np-RhPhCO. The detection limit was calculated to be as low as 9.4 nM, indicating the great potential to detect endogenous H_2S_n in live cells. Importantly, 7 μM Na_2S_2 triggered a prominent enhancement of the fluorescence intensity ratio (I_{486}/I_{591}), while negligible signal fluctuation was obtained in the presence of other analytes (30 μM to 1 mM) (Fig. 3e). Notably, compared with **Np-RhPhCO**, the nanoprobe **PPG-Np-RhPhCO** showed less response towards bulky biothiols and their hydropolysulfides (Cys, GSH, CysSSH and GSSH) even with a longer incubation time (2.5 h) (Fig. 3f and g), which is probably due to physical blocking of the interaction. In addition, **PPG-Np-RhPhCO** is capable of responding toward H_2S_n over a wide pH range (pH 4.0–11.0) (Fig. S12a†).

Another key parameter of ideal fluorescent probes for living cell imaging is stability, primarily including long-term stability and photostability. The formed nano-probe showed good stability with only slight spectral changes for ten days at room temperature (Fig. S13†). Furthermore, illumination with continuous laser scanning showed that the fluorescence signal of **PPG-Np-RhPhCO** remained stable over 3600 s, while the intensity of the parent probe **Np-RhPhCO** decreased by 62 percent, demonstrating the significantly improved photostability of the nano-probe (Fig. 3h). This was ascribed to the fact that the outer polymer micelle provides an effective shelter protecting the inner organic small molecule probe **Np-RhPhCO** from the surrounding environment.[40]

Monitoring endogenous H_2S_n generation in live cells

Inspired by the excellent *in vitro* response, we then investigated the performance of **PPG-Np-RhPhCO** for detecting endogenous generation of H_2S_n in live cells. The cytotoxicity of **PPG-Np-RhPhCO** in cells was first examined by standard MTT assays, indicating negligible cytotoxicity on the human liver cell line HL-7702 (L02) after 24 h of incubation (Fig. S14†). In good agreement with the *in vitro* photostability test, the probe **PPG-Np-RhPhCO** exhibited significantly higher photostability than the parent small-molecule probe **Np-RhPhCO** in live cells under continuous excitation (Fig. S15†). To demonstrate the capability of **PPG-Np-RhPhCO** for detecting endogenous H_2S_n, we next performed live-cell imaging under different stimulation conditions. As shown in Fig. 4a and c, L02 cells incubated with **PPG-Np-RhPhCO** showed weak fluorescence in the green channel (425–475 nm) but strong fluorescence in the red channel (570–620 nm) in the cytosol, indicating a low level of H_2S_n in the normal state. A lower F_{Green}/F_{Red} value was observed when 500 μM *N*-ethylmaleimide (NEM, a RSS blocking agent[32]) was pre-treated for 30 min to cause the depletion of endogenous polysulfide and mercapto compounds. In contrast, addition of

 This journal is © The Royal Society of Chemistry 2020

Open Access Article. Published on 09 July 2020. Downloaded on 2/24/2026 1:23:28 AM.
This article is licensed under a Creative Commons Attribution-NonCommercial 3.0 Unported Licence.

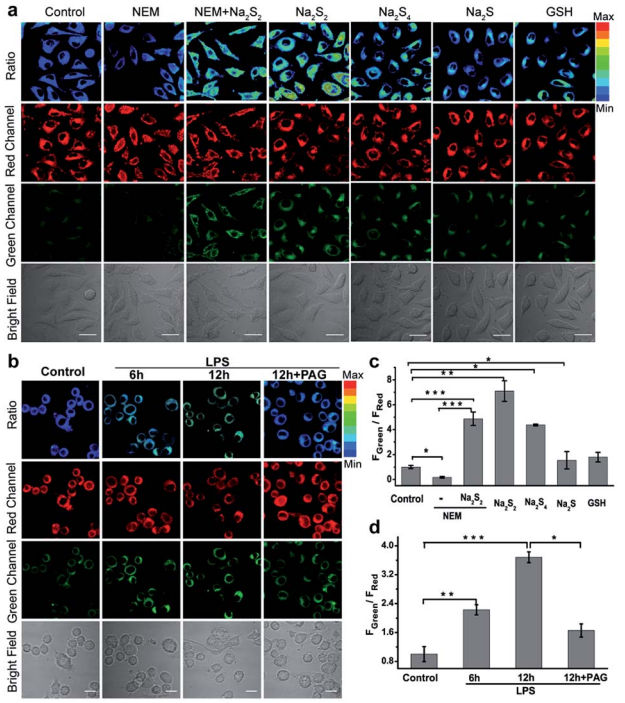

Fig. 4 Imaging exogenous/endogenous H_2S_n with the nano-probe **PPG-Np-RhPhCO** (40 μg mL^{-1}, 4.8 μM). (a) Confocal microscopy images of H_2S_n in live L02 cells with the nano-probe. The first column: incubation with the nano-probe for 2 h; the second column: pretreatment with 500 μM NEM for 0.5 h prior to incubation with the nano-probe for 2 h; the third column: incubation with 30 μM Na_2S_2 for another 20 min after treatment under the conditions in the second column; the fourth to seventh columns: incubation with Na_2S_2 (30 μM), Na_2S_4 (30 μM), Na_2S (50 μM), or GSH (1 mM) for another 20 min, respectively, after treatment with the nano-probe for 2 h. (b) Confocal microscopy images of H_2S_2 in live RAW 264.7 cells with the nano-probe **PPG-Np-RhPhCO** (4.8 μM) after stimulation with LPS. Live RAW 264.7 cells were incubated with the nano-probe for 2 h in the absence and presence of LPS (1 μg mL^{-1}) for 6 h and 12 h, respectively. The fourth column: live RAW 264.7 cells were pretreated with DL-propargylglycine (PAG, 1 mM) for 2 h before incubation with LPS (1 μg mL^{-1}) and probes. (c) Average fluorescence intensity ratios (F_{Green}/F_{Red}) of live L02 cells under the conditions in (a). (d) Average fluorescence intensity ratios (F_{Green}/F_{Red}) of live RAW 264.7 cells under the conditions in (b). Data are mean ± s.e.m., ($n = 5$ independent experiments; 80 cells). Statistical significance was calculated with unpaired two-tailed Student's *t*-tests. *$p < 0.05$, **$p < 0.01$, ***$p < 0.001$. Green channel (425–475 nm), red channel (570–620 nm), pseudocolor ratio images (green channel/red channel). $\lambda_{ex} = 405$ nm. Scale bar: 20 μm.

Na_2S_2 (30 μM) or Na_2S_4 (30 μM), donors of H_2S_n, causes a significant ratiometric signal increase. Notably, 50 μM Na_2S and 1 mM GSH provide only slight F_{Green}/F_{Red} changes, demonstrating the high selectivity of **PPG-Np-RhPhCO** towards H_2S_n in living cells. Next, we further examined the capability of the nano-probe for detecting endogenous H_2S_n generation in RAW 264.7 macrophages. It has been reported that bacterial endotoxin lipopolysaccharide (LPS) can induce the over-expression of cystathionine γ-lyase (CSE), which mediated cysteine metabolism for H_2S_n formation in RAW 264.7 macrophages.[41] Thus, we treated RAW 264.7 macrophages with the probe **PPG-Np-RhPhCO** in the presence of LPS with different incubation times (Fig. 4b and d). It was shown that the fluorescence ratio (F_{Green}/F_{Red}) gradually increased as a function of incubation time, while introduction of 1 mM DL-propargylglycine (PAG, a commercial CSE irreversible inhibitor[42]) yielded a clearly reduced fluorescence ratio signal. Moreover, the capability of the nano-probe **PPG-Np-RhPhCO** for imaging H_2S_n was further confirmed *via* two-photon imaging in live cells, zebrafish, and fresh liver tissues (Fig. S16 and S17†).

H_2S and MPST involved endogenous H_2S_n generation in NAFLD

Nonalcoholic fatty liver disease (NAFLD) is a common type of liver disease that evolves from simple steatosis to hepatitis and liver cancer. Determination of signaling molecules in the process of NAFLD offers insights into disease prevention, drug development and therapeutic evaluation.[14] H_2S has been studied for decades to elucidate its functions in NAFLD;[43,44] however, H_2S_n, as the partner of H_2S coexisting in the organism, has not been investigated in NAFLD due to the lack of suitable probes. Herein, we tried to examine the existence of H_2S_n in NAFLD and further reveal the possible pathway of H_2S_n generation. The NAFLD model was produced *via* incubating normal liver L02 cells with 0.5 mM FFA for 12 h,[45] which was confirmed by the significantly increased lipid droplets and triglycerides based on Oil Red O staining experiments and triglyceride test kits (Fig. S18†). As shown in Fig. 5a and b, treatment with FFA leads to a huge increase in the ratiometric signal ($F_{Green}/F_{Red} = 3.9$), indicating the high level of H_2S_n in NAFLD. Interestingly, an increase of the fluorescence ratio was observed in both normal L02 cells and FFA-stimulated L02 cells when a higher concentration of Na_2S (the donor of H_2S) was produced, indicating that the key role of H_2S is the regulation of endogenous H_2S_n (Fig. 5d). Moreover, a higher level of endogenous H_2S in NFLAD was observed after staining with the reported H_2S probe TPC-N_3 (Fig. S19†),[46] which further suggests a positive correlation between H_2S and H_2S_n production in NAFLD.

Given that both H_2S and H_2S_n can be produced from three major enzymes, CSE, cystathionine-β-synthase (CBS) and 3-mercaptopyruvate sulfurtransferase (MPST),[47–49] the roles of these enzymes in the regulation of production of H_2S_n in FFA-induced NAFLD were examined. As shown in Fig. 5a, a significant reduction of the fluorescence ratio was noted upon addition of pyrrolidine dithiocarbamate (PDTC), which reduced MPST expression by inhibiting the nuclear factor NF-κB/p65.[45] These results were further confirmed by western blot analysis (Fig. 5c). However, pretreatment with PAG (a CSE inhibitor) and aminooxyacetic acid (AOAA, a CBS inhibitor[42]) displayed a negligible change of the fluorescence ratio (Fig. 5a). Therefore, we assumed that MPST participates in the regulation of H_2S_n production in the NAFLD model. The participation of MPST in the regulation of H_2S production under the treatment of FFA was also observed in Li's work.[45] Taken together, we assumed that addition of Na_2S can increase H_2S, the precursor of H_2S_n, thus promoting the further increase of H_2S_n in the NAFLD model. Meanwhile, up-regulation of the expression of MPST stimulated by FFA can also promote the generation of H_2S_n by producing more H_2S or direct reaction with H_2S (Fig. 5d).

Open Access Article. Published on 09 July 2020. Downloaded on 2/24/2026 1:23:28 AM.
This article is licensed under a Creative Commons Attribution-NonCommercial 3.0 Unported Licence.

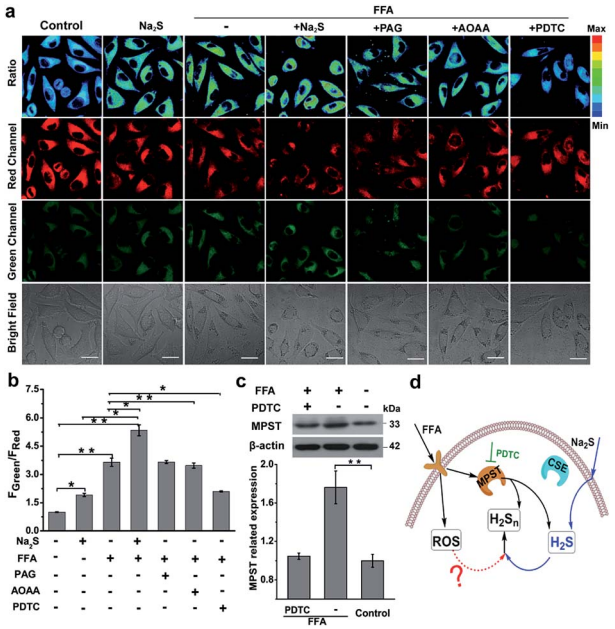

Fig. 5 H_2S_n imaging in NAFLD. (a) Confocal microscopy images of endogenous H_2S_n in L02 cells with the nano-probe **PPG-Np-RhPhCO** (4.8 μM). The first column: incubation with the nano-probe for 2 h; the second column: incubation with 100 μM Na_2S for 1 h before treatment with the nano-probe for 2 h; the third column: incubation with 0.5 mM FFA for 12 h before treatment with the nano-probe for 2 h; the fourth column: incubation with 0.5 mM FFA for 12 h, and then incubation with 100 μM Na_2S for 1 h before treatment with the nano-probe for 2 h; the fifth to seventh columns: pretreatment with AOAA (300 μM), PPG (1 mM), or PDTC (200 μM) for 2 h, respectively, before treatment with 0.5 mM FFA for 12 h and then the nano-probe for 2 h. Green channel (425–475 nm), red channel (570–620 nm), pseudocolor ratio images (green channel/red channel). λ_{ex} = 405 nm. Scale bar: 20 μm. (b) Average fluorescence intensity ratios (F_{Green}/F_{Red}) of live L02 cells under the conditions in (a). Data represent mean standard error ($n = 5$ independent experiments; 60 cells). (c) Western blot analysis showing MPST expression in L02 cells upon treatment with FFA and PDTC, respectively. The MPST relative abundance was normalized with β-actin relative abundance. $n = 3$ independent experiments. Statistical significance was calculated with unpaired two-tailed Student's t-tests. *$p < 0.05$, **$p < 0.01$, ***$p < 0.001$. (d) Proposed schematic of H_2S_n generation in the NAFLD model. Addition of Na_2S can increase H_2S, the precursor of H_2S_n, thus promoting the further increase of H_2S_n in the NAFLD model. Meanwhile, increased MPST expression stimulated by FFA can also promote the generation of H_2S_n by producing more H_2S or direct reaction with H_2S. Black arrows denote the signal pathway in FFA treatment; blue arrows denote the H_2S participational pathway; the red dashed arrow indicates possible ROS effects in the regulation of H_2S_n. PDTC is the MPST inhibitor.

ROS/H_2S/H_2S_n crosstalk signaling pathways in the NAFLD model

Previous literature showed that the reactive oxygen species (ROS) level in NAFLD increases greatly due to the progressive increase of oxidative stress levels caused by mitochondrial abnormalities in hepatic cells.[50] In addition, it is reported that ROS and RNS (including HClO, H_2O_2, $O_2^{\cdot-}$, NO, $ONOO^-$, *etc.*) react with H_2S to form H_2S_n, RSS^-, SO_4^{2-}, SO_3^{2-}, and $S_2O_3^{2-}$;[10,51,52] thus we assumed that higher ROS levels in the NAFLD model would also contribute to production and regulation of H_2S_n (Fig. 5d). Moreover, there is growing evidence that long-term drug use for NAFLD patients could aggravate NAFLD and further increase the level of intracellular ROS.[53–56] Thus, a commonly used drug, acetaminophen (APAP, also known as paracetamol), was chosen to further elucidate the potential pathways of H_2S_n production in a drug-treated NAFLD model.[56,57] As shown in Fig. S21,† both FFA and APAP can lead to higher levels of $ONOO^-$, one of the representative ROS, which was indicated by the reported probe MITO-CC.[58] It was shown that co-treatment with APAP and FFA causes higher ROS production than individual treatment separately (Fig. S20†), probably due to the aggravation of oxidative stress caused by the synergistic effect of APAP and FFA.[56] Significantly, consistent enhancement of H_2S_n and ROS under the above conditions was clearly observed (Fig. 6 and S21†), strongly supporting our assumption that ROS plays an important role in the regulation of H_2S_n production. We also investigated the change of the H_2S_n level *via* two-photon tissue imaging of APAP-treated NAFLD mice, which was consistent with the results of cells imaging (Fig. S22†).

Since we have revealed the function of H_2S in regulation of H_2S_n generation in NAFLD, we next examined the H_2S level changes in the presence of a high concentration of ROS stimulated by APAP and FFA. Interestingly, consistent with ROS level changes, the H_2S level also increased more with co-treatment with FFA and APAP than when treated with FFA or APAP alone (Fig. 6d, S19 and S20†). The consistent variation between ROS and H_2S is probably because of the redox homeostasis in living cells.[59–61] Moreover, treatment with the antioxidant ascorbic acid (VC, a natural, effective antioxidant[62]) in NAFLD greatly reduced H_2S_n, H_2S and ROS levels simultaneously. Taken together, we assumed that direct reaction between H_2S and ROS is probably one of main pathways for producing H_2S_n, forming a ROS/H_2S/H_2S_n crosstalk signaling pathway.

To further explore the functions of enzymes CSE, MPST and CBS in regulating the ROS/H_2S/H_2S_n pathway, PAG (inhibitor of CSE), PDTC (inhibitor of MPST), and AOAA (inhibitor of CBS) were treated, respectively, prior to imaging H_2S_n in APAP and FFA-treated L02 cells (Fig. 6a and b). Both H_2S_n and H_2S displayed a significant decrease in the presence of PAG or PDTC, which points to the capability of CSE and MPST in regulating H_2S_n and H_2S in the NAFLD model. However, the inhibitor AOAA had no obvious inhibitory effects maybe because the abundance of CBS in the liver is much lower than that of CSE.[63] These results were also consistent with the CSE and MPST western blot analysis results (Fig. 6c). Thus, the consistent changes of H_2S and H_2S_n by regulation of CSE and MPST allow us to confirm the roles of H_2S, CSE and MPST in the H_2S_n generation pathways (Fig. 6e). In combination with the participation of ROS in regulation of H_2S_n generation, we proposed the ROS/H_2S/H_2S_n crosstalk signaling pathways in Fig. 6e. Increased ROS in FFA-induced NAFLD stimulates MPST and CSE to produce more H_2S, which causes enhancement of H_2S_n *via* direct reaction with ROS or catalysis by MPST and CSE.

In this work, to accurately and selectively image the intracellular H_2S_n, we introduced a new ratiometric fluorescent

This journal is © The Royal Society of Chemistry 2020

Open Access Article. Published on 09 July 2020. Downloaded on 2/24/2026 1:23:28 AM.
This article is licensed under a Creative Commons Attribution-NonCommercial 3.0 Unported Licence.

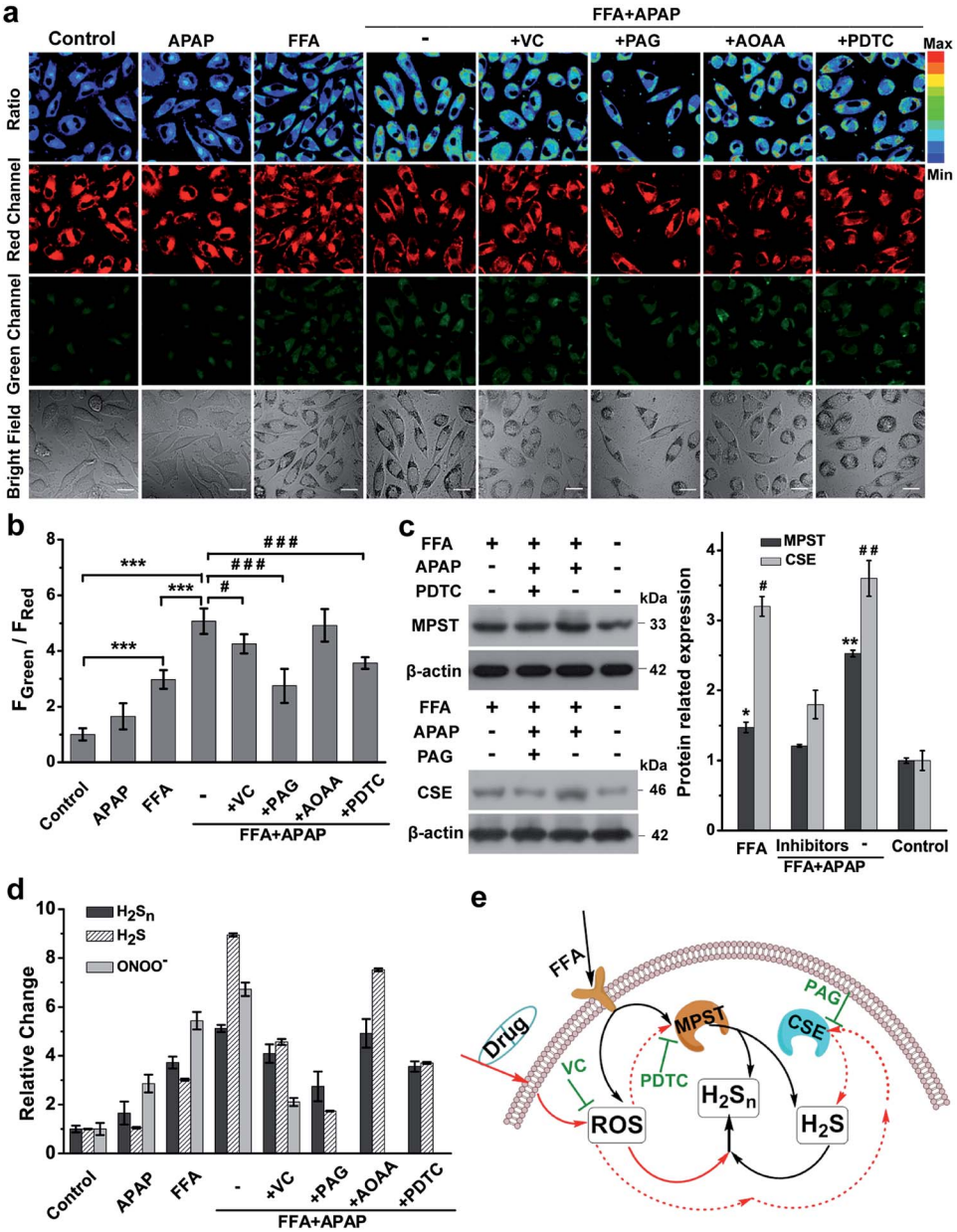

Fig. 6 H_2S_n imaging in drug-treated NAFLD. (a) Confocal fluorescence images of the nano-probe **PPG-Np-RhPhCO** (4.8 μM) in L02 cells under different conditions. The first column: incubation with the nano-probe for 2 h prior to imaging; the second and third columns: incubation with the nano-probe for 2 h after treatment with APAP (3 mM) or FFA (0.5 mM) for 12 h, respectively. The fourth to eighth columns: treatment with FFA (0.5 mM) for 12 h and VC (1 mM), PAG (1 mM), AOAA (300 μM) or PDTC (200 μM) for 2 h, respectively, and then with APAP (3 mM) for 12 h and with the nano-probe for 2 h. Green channel (425–475 nm), red channel (570–620 nm), pseudocolor ratio images (green channel/red channel). λ_{ex} = 405 nm. Scale bar: 20 μm. (b) Average fluorescence intensity ratios (F_{Green}/F_{Red}) of live L02 cells under the conditions in (a). Data represent mean standard error ($n = 5$ independent experiments; 80 cells). Statistical significance in (a) was calculated with unpaired two-tailed Student's *t*-tests. ***$p < 0.001$. Significance is expressed as $^{\#}$ compare to the co-treatment with FFA and APAP, $^{\#}p < 0.05$, $^{\#\#\#}p < 0.001$. (c) Western blot analysis showing MPST and CSE expression in L02 cells upon treatment with FFA, APAP and inhibitor (PDTC or PAG), respectively. The MPST and CSE relative abundance was normalized with β-actin relative abundance. $n = 3$ independent experiments. (d) The relative levels of $ONOO^-$, H_2S and H_2S_n in the NAFLD model. The data were based on fluorescence imaging of L02 cells stained with $ONOO^-$, H_2S and H_2S_n probes (MITO-CC in Fig. S21,† TPC-N_3 in Fig. S20† and **PPG-Np-RhPhCO** in Fig. 6a), respectively, and were normalized with their respective control group. (e) Schematic of ROS/H_2S/H_2S_n crosstalk signaling pathways that regulate H_2S_n generation in the NAFLD model. Increased ROS in FFA-induced NAFLD stimulate MPST and CSE to produce more H_2S, which causes enhancement of H_2S_n *via* direct reaction with ROS or catalysis by MPST and CSE. Black arrows denote the H_2S_n generation pathway in FFA-induced NAFLD; red solid arrows and dashed arrows indicate ROS roles in the regulation of H_2S_n in drug-treated NAFLD, respectively. VC represents antioxidants while PDTC and PAG indicate MPST and CSE inhibitors, respectively.

Open Access Article. Published on 09 July 2020. Downloaded on 2/24/2026 1:23:28 AM. This article is licensed under a Creative Commons Attribution-NonCommercial 3.0 Unported Licence.

probe **PPG-Np-RhPhCO**, characterized by three main features that distinguish it from previous H_2S_n sensors. First, rational design and fast screening offer new recognition sites for sensing H_2S_n, which avoid interference of pH and hydrolases in living cells. Second, introduction of nanoparticles formed by polymers enables the further improvement of selectivity of the probe, which is a prerequisite for applications in complex biological environments and a bottleneck for most small-molecule fluorescent probes. The encapsulation of fluorophores into nanoparticles works as a general method to improve the selectivity because it avoids the interaction with bulky potential competitors (Cys, GSH, CysSSH and GSSH), which were main interferences for previous H_2S_n probes. Third, the nano-probe can offer more accurate detection of H_2S_n through ratiometric imaging in living cells. The ratiometric quantification calculated from two signal channels can exclude the interference of probe concentration, which particularly benefits cell imaging under different stimulation conditions.

To examine the application of the new H_2S_n probe in live-cell imaging, we incubated **PPG-Np-RhPhCO** with the liver cell line, HL-7702 cells, and murine macrophage cell line, RAW 264.7 cells. Live-cell imaging demonstrated the capability of the probe in detecting endogenous H_2S_n with good sensitivity and signal to background ratio (Fig. 4). The excellent performance of this probe in imaging and monitoring H_2S_n inspired us to address the challenge of H_2S_n production pathways. In the NAFLD model, we found that FFA could stimulate MPST expression, which promotes the generation of H_2S_n. Moreover, as the precursor, H_2S at higher concentration can promote the further increase of H_2S_n in the NAFLD model. To further explore the roles of ROS in the production of H_2S_n, we introduced a widely used drug, APAP, to boost ROS production in the NAFLD model. Simultaneous treatment with APAP and FFA causes a dramatic increase of ROS, which stimulates MPST and CSE to increase the generation of H_2S to maintain redox homeostasis. It is also worth noting that higher expression of CSE in L02 cells was observed under the treatment with FFA and APAP simultaneously, but not under treatment with FFA alone. This is probably because ROS at very high levels can stimulate CSE upregulation to elevate the level of antioxidant H_2S to maintain the redox balance.[64] A higher level of ROS and H_2S can generate more H_2S_n *via* chemical reaction, forming one of main pathways for H_2S_n production in NAFLD. Meanwhile, MPST and CSE which are highly expressed under FFA and APAP-stimulation can also directly induce H_2S to generate H_2S_n, forming another main pathway for H_2S_n production in NAFLD. The ROS/H_2S/H_2S_n pathways in the NAFLD model (Fig. 6e) reported in this work will provide new insights into future drug development and therapeutic evaluation for NAFLD patients.

Conclusions

In summary, we designed and developed a ratiometric fluorescent probe, **PPG-Np-RhPhCO**, for monitoring the generation of endogenous H_2S_n in NAFLD. The new probe, **PPG-Np-RhPhCO**, was successfully applied to reveal the possible ROS/H_2S/H_2S_n pathways in the NAFLD model. The excellent selectivity, photostability and biocompatibility of the probe **PPG-Np-RhPhCO** enable it to be a practical and direct tool for detecting and studying intracellular H_2S_n in complex biological samples.

Ethical statement

All animal procedures were performed in accordance with the Guidelines for Care and Use of Laboratory Animals of Hunan University, and all animal experiments were approved by the Animal Ethics Committee of the College of Biology (Hunan University).

Conflicts of interest

There are no conflicts to declare.

Acknowledgements

This work was supported by the National Science Foundation of China (21877029, 21735001, and 21622504) and the National Key R&D Program of China (2019YFA0210103). We thank Dr W. Chen and Prof. M. Xian (Washington State University) for supplying Na_2S_2 and Na_2S_4.

Notes and references

1 M. R. Filipovic, J. Zivanovic, B. Alvarez and R. Banerjee, *Chem. Rev.*, 2017, **118**, 1253–1337.
2 M. Yang, J. Fan, J. Du and X. Peng, *Chem. Sci.*, 2020, **11**, 5127–5141.
3 G. I. Giles, K. M. Tasker and C. Jacob, *Free Radical Biol. Med.*, 2001, **31**, 1279–1283.
4 C. Liu, W. Chen, W. Shi, B. Peng, Y. Zhao, H. Ma and M. Xian, *J. Am. Chem. Soc.*, 2014, **136**, 7257–7260.
5 R. Greiner, Z. Pálinkás, K. Bäsell, D. Becher, H. Antelmann, P. Nagy and T. P. Dick, *Antioxid. Redox Signaling*, 2013, **19**, 1749–1765.
6 H. Kimura, *Proc. Jpn. Acad., Ser. B*, 2015, **91**, 131–159.
7 H. Kimura, *Nitric Oxide*, 2014, **41**, 4–10.
8 D. Zhang, I. Macinkovic, N. O. Devarie-Baez, J. Pan, C. M. Park, K. S. Carroll, M. R. Filipovic and M. Xian, *Angew. Chem., Int. Ed.*, 2014, **53**, 575–581.
9 H. Kimura, *Molecules*, 2014, **19**, 16146.
10 K. Hideo, *Antioxid. Redox Signaling*, 2017, **27**, 619–621.
11 M. C. Gruhlke and A. J. Slusarenko, *Plant Physiol. Biochem.*, 2012, **59**, 98–107.
12 J. Zhang, X. Y. Zhu, X. X. Hu, H. W. Liu, J. Li, L. L. Feng, X. Yin, X. B. Zhang and W. Tan, *Anal. Chem.*, 2016, **88**, 11892–11899.
13 N. E. Francoleon, S. J. Carrington and J. M. Fukuto, *Arch. Biochem. Biophys.*, 2011, **516**, 146–153.
14 N. Berndt, S. Bulik, I. Wallach, T. Wünsch, M. König, M. Stockmann, D. Meierhofer and H. G. Holzhütter, *Nat. Commun.*, 2018, **9**, 2386.
15 S. K. Erickson, *J. Lipid Res.*, 2009, **50**, S412–S416.
16 K. Namekata, Y. Enokido, I. Ishii, Y. Nagai, T. Harada and H. Kimura, *J. Biol. Chem.*, 2004, **279**, 52961–52969.

 This journal is © The Royal Society of Chemistry 2020

Open Access Article. Published on 09 July 2020. Downloaded on 2/24/2026 1:23:28 AM.
This article is licensed under a Creative Commons Attribution-NonCommercial 3.0 Unported Licence.

17 S. Mani, G. Yang and R. Wang, *Free Radical Biol. Med.*, 2011, **50**, 1280–1287.
18 C. M. Park, L. Weerasinghe, J. J. Day, J. M. Fukuto and M. Xian, *Mol. BioSyst.*, 2015, **11**, 1775–1785.
19 P. Gao, W. Pan, N. Li and B. Tang, *Chem. Sci.*, 2019, **10**, 6035–6071.
20 W. Chen, E. W. Rosser, T. Matsunaga, A. Pacheco, T. Akaike and M. Xian, *Angew. Chem., Int. Ed.*, 2015, **54**, 13961–13965.
21 Y. Hou, X. F. Yang, Y. Zhong and Z. Li, *Sens. Actuators, B*, 2016, **232**, 531–537.
22 K. Umezawa, M. Kamiya and Y. Urano, *Angew. Chem., Int. Ed.*, 2018, **57**, 9346–9350.
23 R. Kawagoe, I. Takashima, S. Uchinomiya and A. Ojida, *Chem. Sci.*, 2017, **8**, 1134–1140.
24 Y. Takano, K. Hanaoka, K. Shimamoto, R. Miyamoto, T. Komatsu, T. Ueno, T. Terai, H. Kimura, T. Nagano and Y. Urano, *Chem. Commun.*, 2017, **53**, 1064–1067.
25 F. Yu, M. Gao, M. Li and L. Chen, *Biomaterials*, 2015, **63**, 93–101.
26 L. Zeng, S. Chen, T. Xia, W. Hu, C. Li and Z. Liu, *Anal. Chem.*, 2015, **87**, 3004–3010.
27 E. Cuevasanta, M. N. Moller and B. Alvarez, *Arch. Biochem. Biophys.*, 2017, **617**, 9–25.
28 E. Cuevasanta, M. Lange, J. Bonanata, E. L. Coitino, G. Ferrer-Sueta, M. R. Filipovic and B. Alvarez, *J. Biol. Chem.*, 2015, **290**, 26866–26880.
29 L. Yuan, W. Lin, K. Zheng and S. Zhu, *Acc. Chem. Res.*, 2013, **46**, 1462–1473.
30 M. H. Lee, J. S. Kim and J. L. Sessler, *Chem. Soc. Rev.*, 2015, **44**, 4185–4191.
31 W. Li, S. Yin, X. Gong, W. Xu, R. Yang, Y. Wan, L. Yuan and X. B. Zhang, *Chem. Commun.*, 2020, **56**, 1349–1352.
32 Q. Han, Z. Mou, H. Wang, X. Tang, Z. Dong, L. Wang, X. Dong and W. Liu, *Anal. Chem.*, 2016, **88**, 7206–7212.
33 W. Lin, L. Yuan, Z. Cao, Y. Feng and J. Song, *Angew. Chem., Int. Ed.*, 2010, **49**, 375–379.
34 L. Zhou, X. Zhang, Q. Wang, Y. Lv, G. Mao, A. Luo, Y. Wu, Y. Wu, J. Zhang and W. Tan, *J. Am. Chem. Soc.*, 2014, **136**, 9838–9841.
35 M. De, P. S. Ghosh and V. M. Rotello, *Adv. Mater.*, 2008, **20**, 4225–4241.
36 K. Li and B. Liu, *Chem. Soc. Rev.*, 2014, **43**, 6570–6597.
37 H. N. Kim, Z. Guo, W. Zhu, J. Yoon and H. Tian, *Chem. Soc. Rev.*, 2011, **40**, 79–93.
38 L. Chen, S. Xu, W. Li, T. Ren, L. Yuan, S. Zhang and X. B. Zhang, *Chem. Sci.*, 2019, **10**, 9351–9357.
39 L. Wu, Y. Sun, K. Sugimoto, Z. Luo, Y. Ishigaki, K. Pu, T. Suzuki, H. Y. Chen and D. Ye, *J. Am. Chem. Soc.*, 2018, **140**, 16340–16352.
40 J. Yan, M. C. Estévez, J. E. Smith, K. Wang, X. He, L. Wang and W. Tan, *Nano Today*, 2007, **2**, 44–50.
41 X. Y. Zhu, S. J. Liu, Y. J. Liu, S. Wang and X. Ni, *Cell. Mol. Life Sci.*, 2010, **67**, 1119–1132.
42 A. Asimakopoulou, P. Panopoulos, C. T. Chasapis, C. Coletta, Z. Zhou, G. Cirino, A. Giannis, C. Szabo, G. A. Spyroulias and A. Papapetropoulos, *Br. J. Pharmacol.*, 2013, **169**, 922–932.
43 Z. L. Luo, L. J. Tang, T. Wang, R. W. Dai, J. D. Ren, L. Cheng, K. Xiang and F. Z. Tian, *J. Gastroenterol. Hepatol.*, 2014, **29**, 215–222.
44 K. S. Lindsei, L. S. Yaw and O. Karmin, *Can. J. Physiol. Pharmacol.*, 2015, **93**, 1–11.
45 M. Li, C. Xu, J. Shi, J. Ding, X. Wan, D. Chen, J. Gao, C. Li, J. Zhang, Y. Lin, Z. Tu, X. Kong, Y. Li and C. Yu, *Gut*, 2018, **67**, 2169–2180.
46 T. B. Ren, W. Xu, Q. L. Zhang, X. X. Zhang, S. Y. Wen, H. B. Yi, L. Yuan and X. B. Zhang, *Angew. Chem., Int. Ed.*, 2018, **57**, 7473–7477.
47 S. Yuan, X. Shen and C. G. Kevil, *Antioxid. Redox Signaling*, 2017, **27**, 634–653.
48 N. Shibuya, M. Tanaka, M. Yoshida, Y. Ogasawara, T. Togawa, K. Ishii and H. Kimura, *Antioxid. Redox Signaling*, 2008, **11**, 703–714.
49 T. Ida, T. Sawa, H. Ihara, Y. Tsuchiya, Y. Watanabe, Y. Kumagai, M. Suematsu, H. Motohashi, S. Fujii, T. Matsunaga, M. Yamamoto, K. Ono, N. O. Devarie-Baez, M. Xian, J. M. Fukuto and T. Akaike, *Proc. Natl. Acad. Sci. U. S. A.*, 2014, **111**, 7606–7611.
50 A. Borrelli, P. Bonelli, F. M. Tuccillo, I. D. Goldfine, J. L. Evans, F. M. Buonaguro and A. Mancini, *Redox Biol.*, 2018, **15**, 467–479.
51 B. L. Predmore, D. J. Lefer and G. Gojon, *Antioxid. Redox Signaling*, 2012, **17**, 119–140.
52 M. M. Cortese-Krott, G. G. C. Kuhnle, A. Dyson, B. O. Fernandez, M. Grman, J. F. DuMond, M. P. Barrow, G. McLeod, H. Nakagawa, K. Ondrias, P. Nagy, S. B. King, J. E. Saavedra, L. K. Keefer, M. Singer, M. Kelm, A. R. Butler and M. Feelisch, *Proc. Natl. Acad. Sci. U. S. A.*, 2015, **112**, 4651–4660.
53 B. Fromenty, *J. Hepatol.*, 2013, **58**, 824–826.
54 M. A. Robin, I. Sauvage, T. Grandperret, V. Descatoire, D. Pessayre and B. Fromenty, *FEBS Lett.*, 2005, **579**, 6895–6902.
55 S. Donthamsetty, V. S. Bhave, M. S. Mitra, J. R. Latendresse and H. M. Mehendale, *Hepatology*, 2007, **45**, 391–403.
56 A. Michaut, C. Moreau, M. A. Robin and B. Fromenty, *Liver Int.*, 2014, **34**, 171–179.
57 G. Tarantino, P. Conca, V. Basile, A. Gentile, D. Capone, G. Polichetti and E. Leo, *Hepatol. Res.*, 2007, **37**, 410–415.
58 D. Cheng, Y. Pan, L. Wang, Z. Zeng, L. Yuan, X. Zhang and Y. T. Chang, *J. Am. Chem. Soc.*, 2017, **139**, 285–292.
59 K. R. Olson and Y. Gao, *Free Radical Biol. Med.*, 2019, **135**, 1–14.
60 Y. Kimura, R. Dargusch, D. Schubert and H. Kimura, *Antioxid. Redox Signaling*, 2006, **8**, 661–670.
61 Z. S. Xu, X. Y. Wang, D. M. Xiao, L. F. Hu, M. Lu, Z. Y. Wu and J. S. Bian, *Free Radical Biol. Med.*, 2011, **50**, 1314–1323.
62 A. E. Wagner, P. Huebbe, T. Konishi, M. M. Rahman, M. Nakahara, S. Matsugo and G. Rimbach, *J. Agric. Food Chem.*, 2008, **56**, 11694–11699.
63 P. Manna, N. Gungor, R. McVie and S. K. Jain, *J. Biol. Chem.*, 2014, **289**, 11767–11778.
64 Y. Pan, S. Ye, D. Yuan, J. Zhang, Y. Bai and C. Shao, *Mutat. Res.*, 2012, **738–739**, 12–18.